Tanshinone IIA targets RNF123 to inhibit non-small cell lung cancer cell proliferation, migration and invasion via KAT2B-mediated H3K18ac modification

YONGJIE HE, YINGXIN ZHANG, JIANGSHENG ZHANG and KAICAN CAI

Department of Thoracic Surgery, Nanfang Hospital, Southern Medical University, Guangzhou, Guangdong 510515, P.R. China

Received October 25, 2024; Accepted November 7, 2025

DOI: 10.3892/ol.2025.15422

Abstract. Tanshinone IIA (TSIIA) exerts antitumor effects. The present study aimed to explore the pharmacological effect of TSIIA on lung cancer development and assess the potential underlying mechanism of action. Cell viability and proliferation were assessed using Cell Counting Kit-8 and 5-ethynyl-20-deoxyuridine assays, respectively. Transwell assays were performed to determine cell migration and invasion. Histone H3 lysine 18 acetylation (H3K18ac) and histone H4 lysine 8 acetylation (H4K8ac) enrichment in the RING finger protein 123 (RNF123) promoter and the interaction between lysine acetyltransferase 2B (KAT2B) and the RNF123 promoter were analyzed by chromatin immunoprecipitation assays. The results indicated that RNF123 was weakly expressed in lung cancer cells, and its upregulation decreased lung cancer cell viability, proliferation, migration, invasion and epithelial-mesenchymal transition. Sodium TSIIA sulfate (STS) treatment inhibited the non-small cell lung cancer (NSCLC) cell malignant phenotypes, which were reversed by the knockdown of RNF123. Mechanistically, TSIIA promoted KAT2B-mediated H3K18ac modification at the promoter region of the RNF123 gene, leading to upregulated RNF123 expression in NSCLC cells. Additionally, KAT2B knockdown prevented the STS-induced inhibition of NSCLC cell malignant phenotypes. Furthermore, RNF123 upregulation restored the effect of KAT2B knockdown on STS-treated NSCLC phenotypes. In conclusion, TSIIA inhibited the NSCLC cell malignant phenotypes via the epigenetic modification of RNF123.

Correspondence to: Dr Kaican Cai, Department of Thoracic Surgery, Nanfang Hospital, Southern Medical University, 1838 North Guangzhou Avenue, Guangzhou, Guangdong 510515, P.R. China
E-mail: doc_cai@163.com

Abbreviations: NSCLC, non-small cell lung cancer; LUAD, lung adenocarcinoma; LUSC, lung squamous cell carcinoma; TSIIA, tanshinone IIA; STS, sodium TSIIA sulfate; HAT, histone acetyltransferase; HDAC, histone deacetylase; RNF123, RING finger protein 123; KAT2B, lysine acetyltransferase 2B; RT-qPCR, reverse transcription-quantitative PCR; CCK-8, Cell Counting Kit-8; EdU, 5-ethynyl-20-deoxyuridine; ChIP, chromatin immunoprecipitation; H3K18ac, acetylation of histone H3 lysine 18 site; H4K8ac, acetylation of histone H4 lysine 8 site

Key words: NSCLC cells, TSIIA, RNF123, KAT2B, histone acetylation

Introduction

Lung cancer is the most frequently diagnosed malignant tumor and a major cause of cancer-related death globally (1). Non-small cell lung cancer (NSCLC) constitutes >85% of all lung cancer cases, which can be further classified as lung adenocarcinoma (LUAD), large cell carcinoma and lung squamous cell carcinoma (LUSC) (2,3). In recent years, surgery, chemotherapy and medication have been the main treatment strategies for lung cancer, but the prognosis for patients with this disease remains poor (3). To improve patient survival, the development of new anticancer drugs with lower toxicity and fewer side effects are required for the treatment of lung cancer.

Tanshinone IIA (TSIIA) is a natural extract derived from Danshen (*Salviae miltiorrhizae* Bunge). Sodium TSIIA sulfate (STS) is an aqueous solution of TSIIA after sulfonation and is the sodium sulfate salt form of TSIIA. Compared with the lipophilic properties of TSIIA, the introduction of the sulfate group in STS enhances its solubility in aqueous media, which improves its absorption and distribution within the body. Despite the structural differences between the molecules, STS, as a derivative of TSIIA, retains certain pharmacological activities of TSIIA, such as anti-inflammatory, antioxidant and antitumor effects (4). As previously reported, TSIIA exerts antitumor effects on various malignant tumors, such as esophageal, colorectal, prostate and gastric cancer (4,5). Notably, the therapeutic effects of TSIIA on lung cancer have been reported, and TSIIA markedly decreases NSCLC cell viability and colony formation (6). In addition, STS treatment has been shown to reduce LUAD cell malignant behaviors (7). However, the precise mechanism by which TSIIA functions in lung cancer remains unclear.

Histone acetylation is a specific type of modification in which the lysine residue at the tail of a histone is acetylated and deacetylated by histone acetyltransferase (HAT) and histone deacetylase (HDAC), respectively (8). Alterations in histone acetylation are closely related to cancer progression (9). For instance, upregulation of histone H3 lysine 18 acetylation

(H3K18ac) inhibits lung cancer cell viability, colony formation and migration (10). Additionally, celestrol inhibits lung cancer growth by inducing histone acetylation and synergistically acting with a HDAC inhibitor (11). As previously reported, TSIIA protects against cerebral ischemia reperfusion injury by upregulating H3K18ac and H4K8ac (12). Therefore, it could be suggested that TSIIA may inhibit lung cancer development by upregulating H3K18ac and H4K8ac.

RING finger protein 123 (RNF123), also known as KPC1, is an E3 ubiquitin ligase component of the ubiquitin-proteasome system that controls certain important cancer pathways and processes (13). The tumor suppressor functions of RNF123 have been previously reported (13). RNF123 is expressed at low levels in glioblastoma tumors and its low expression is a predictive factor for poor overall survival (14). Nevertheless, at present, the role of RNF123 in lung cancer is not well understood. To address this gap, the present study aimed to identify a possible novel therapy for lung cancer and elucidate its mechanism of action by investigating RNF123 expression in LUAD and LUSC and assessing the potential role of promoter histone acetylation (H3K18ac, H4K8ac and H3K27ac) in regulating its transcription using bioinformatic methods.

Materials and methods

Cell culture and treatment. The A549, H1975, H1299, H460 and PC-9 lung cancer cell lines and the BEAS-2B normal human bronchial epithelial cell line were obtained from ATCC. All cells were cultured in RPMI 1640 (Gibco; Thermo Fisher Scientific, Inc.) comprising 10% FBS (Gibco Fisher Scientific, Inc.) with 5% CO_2 at 37˚C. For STS treatment, A549 and H1975 cells were incubated with 0, 5, 10, 20, 40 and 80 μM STS (Sigma-Aldrich; Merck KGaA) for 24 h.

Cell transfection. The short hairpin RNAs [shRNAs; sh-negative control (NC) sense, 5'-GTTCTCCGAACGTGTCACGT-3' and antisense, 5'-ACGTGACACGTTCGGAGAAC-3'; sh-RNF123 sense, 5'-CCCTCAAAGATGACCTTGCTT-3' and antisense, 5'-AAGCAAGGTCATCTTTGAGGG-3'; and sh-lysine acetyltransferase 2B (KAT2B) sense, 5'-GCTGGGACAATTTCA TACAA-3' and antisense, 5'-TTGTATGAAATTGTCCCA GC-3'], the overexpression (oe) plasmids (oe-RNF123 and oe-KAT2B), pCDNA3.1-CMV-RNF123 (human)-GFP-Neo and pCDNA3.1-CMV-KAT2B (human)-GFP-Neo, and their respective negative controls (empty pCDNA3.1 vector) were purchased from Shanghai GenePharma Co., Ltd. The overexpression vectors and shRNAs were transfected into cells using Lipofectamine 3000 (Invitrogen; Thermo Fisher Scientific, Inc.). Briefly, 2.5 μg of nucleic acid was used per well of a 6-well plate. Transfection complexes were formed at room temperature for 15 min and then added to cells, which were incubated at 37˚C with 5% CO_2. Cells were incubated for 48 h post-transfection before subsequent experimentation. In addition to sh-NC and oe-NC controls, mock-transfected control cells (cultured in parallel with transfection reagent only, without nucleic acid) were included in all assays to serve as the baseline control group.

Reverse transcription-quantitative PCR (RT-qPCR). Total RNA was extracted from A549 and H1975 cells using TRIzol (Invitrogen; Thermo Fisher Scientific, Inc.). cDNA synthesis was carried out using the SuperScript™ IV First-Strand Synthesis System (Thermo Fisher Scientific, Inc.) according to the manufacturer's protocol. qPCR was performed using the PowerUp™ SYBR™ Green Master Mix (Thermo Fisher Scientific, Inc.) on a QuantStudio™ 3 Real-Time PCR System with the following thermocycling conditions: Initial denaturation at 95˚C for 2 min, followed by 40 cycles of 95˚C for 15 sec and 60˚C for 1 min, with a final melting curve analysis from 65˚C to 95˚C.GAPDH was employed as the reference gene. The data were analyzed using the $2^{-\Delta\Delta Cq}$ method (15). The primers used in the present study were as follows: RNF123 forward (F), 5'-TCTTTCTCCCGCAAGAGCTAT-3' and reverse (R), 5'-AACTGGTCCAAATGTTCTGGC-3'; KAT2B F, 5'-CGA ATCGCCGTGAAGAAAGC-3' and R, 5'-CTTGCAGGCG GAGTACACT-3'; and GAPDH F, 5'-AGGTCGGAGTCAACG GATTT-3' and R, 5'-TGACGGTGCCATGGAATTTG-3'.

Western blotting. For nuclear extraction, cells were lysed in hypotonic buffer (10 mM HEPES pH 7.9, 10 mM KCl, 1.5 mM $MgCl_2$, 0.1% NP-40, protease inhibitors) on ice for 15 min, nuclei were pelleted at 3,000 x g for 5 min at 4˚C, washed once with hypotonic buffer without NP-40 and then extracted with high-salt buffer (20 mM HEPES pH 7.9, 420 mM NaCl, 1.5 mM $MgCl_2$, 0.2 mM EDTA, 25% glycerol, protease inhibitors) for 30 min at 4˚C with rotation. A BCA kit (Thermo Fisher Scientific, Inc.) was used to measure the proteins after they had been isolated using RIPA (Beyotime Institute of Biotechnology). The total protein (10 μg per lane) was separated by 10% SDS-PAGE and transferred to a PVDF membrane (MilliporeSigma). The membranes were blocked with 5% non-fat milk (Amresco, LLC; cat. no. GRM1254-500G) in TBST (0.1% Tween-20) for 1 h at room temperature, then incubated overnight at 4˚C with primary antibodies purchased from Abcam against RNF123 (cat. no. ab221877; 1:1,000), H3 (cat. no. ab1791; 1:10,000), H4 (cat. no. ab31830; 1:5,000), H3K18ac (cat. no. ab40888; 1:500), H4K8ac (cat. no. ab45166; 1:500), H3K27ac (cat. no. ab4729; 1:1,000), KAT2B (cat. no. ab96510; 1:1,000), E-cadherin (cat. no. ab227639; 1:2,000), Vimentin (cat. no. ab92547; 1:1,000) and GAPDH (cat. no. ab9485; 1:5,000). The membranes were then incubated with the horseradish peroxidase-conjugated anti-rabbit secondary antibody (cat. no. ab7090; Abcam; 1:5,000) and anti-mouse secondary antibody (cat. no. ab97023; Abcam; 1:5,000) for 60 min at room temperature. The protein bands were visualized using ECL (cat. no. P10060; NCM Biotech; Suzhou Xinsaimei Biotechnology Co., Ltd.) and semi-quantified using ImageJ software (version 1.80; National Institutes of Health). For normalization, the ratio of the grayscale value of the target protein to that of the loading control was calculated for each sample. The relative expression level of the target protein was determined using the following formula: Relative expression (%)=(target protein grayscale value/loading control grayscale value) x100.

Cell Counting Kit-8 (CCK-8) assay. Cells were cultured in 24-well plates (1x10^4 cells/well) for 24 h. Cells were then treated for 3 h with 10 μl CCK-8 solution (Yeason Biotechnology). Subsequently, the absorbance at 450 nm was measured.

5-ethynyl-20-deoxyuridine (EdU) assay. Cells were seeded into confocal plates (1x10^6 cells/well) and incubated with 50 μM

EdU buffer for 2 h (Guangzhou RiboBio Co., Ltd.). Cells were then fixed with 4% paraformaldehyde in PBS for 15 min at room temperature and permeabilized with 0.5% Triton X-100 in PBS for 20 min at room temperature. After adding EdU solution to the culture, the nuclei were stained with Hoechst for 15 min at room temperature in the dark. The samples were imaged using an Olympus fluorescence microscope. EdU-positive cells were quantified using ImageJ software.

Transwell assay. DMEM (cat. no. 11965092; Thermo Fisher Scientific, Inc.) containing $1x10^4$ cells (500 μl) was added to the upper chamber of a Transwell plate precoated with Matrigel (1:8 ratio; Corning, Inc.) at 37˚C for 4 h for invasion assays. Migration assays were performed using uncoated Transwell plates. Complete DMEM (1,000 μl) was added to the lower chamber. Cells in the upper chamber were removed after incubation at 37˚C for 12 h, while cells in the lower chamber were fixed with 4% paraformaldehyde for 20 min at room temperature and stained with 0.5% crystal violet for 20 min at room temperature. An Olympus light microscope was used to image the cells. DMEM was selected instead of RPMI 1640 as A549 and H1975 cells exhibited optimal growth and migration in DMEM based on preliminary optimization.

Chromatin immunoprecipitation (ChIP) assay. Using a pre-prepared confluent 10 cm dish (~10^7 cells), the cells were fixed with 1% formaldehyde for 5 min at room temperature to induce DNA-protein cross-linking. Cell lysate was then sonicated on ice for 15 min (30 sec on/30 sec off cycles at 20% amplitude) to produce chromatin fragments and incubated overnight with anti-H3K18ac (cat. no. ab40888; 1:500; Abcam), anti-H4K8ac (cat. no. ab45166; 1:200; Abcam), anti-KAT2B (cat. no. ab96510; 1:100; Abcam) or anti-IgG (cat. no. ab172730; 1:100; Abcam) antibodies. Pierce protein A/G magnetic beads (Thermo Fisher Scientific, Inc.; 30 μl bead slurry per reaction) were incubated with the chromatin-antibody mixture for 4 h at 4˚C with rotation. Beads were collected on a magnetic rack and washed sequentially at 4˚C with 1 ml each of low-salt buffer (20 mM Tris-HCl pH 8.0, 150 mM NaCl, 2 mM EDTA, 1% Triton X-100), high-salt buffer (20 mM Tris-HCl pH 8.0, 500 mM NaCl, 2 mM EDTA, 1% Triton X-100), LiCl buffer (10 mM Tris-HCl pH 8.0, 250 mM LiCl, 1 mM EDTA, 1% NP-40, 1% sodium deoxycholate) and TE buffer (10 mM Tris-HCl pH 8.0, 1 mM EDTA). Each wash step included rotation for 5 min at 4˚C followed by centrifugation at 1,000 x g for 1 min at 4˚C. The chromatin-antibody complexes were eluted by incubating the beads in 200 μl elution buffer (1% SDS, 100 mM $NaHCO_3$) at 65˚C for 30 min with frequent vortexing. DNA was purified using the QIAquick PCR Purification Kit (cat. no. 28106; Qiagen Diagnostics) according to the manufacturer's instructions and analyzed using RT-qPCR with primers specific for the RNF123 promoter region (forward: 5'-GCA TCTGTGTGGTCCTGACA-3'; and reverse: 5'-TCTTGAGCA CAGCTGGGAAG-3').

Data retrieval and statistical analysis. The StarBase database (http://starbase.sysu.edu.cn/) was used to retrieve and analyze the expression levels of RNF123 and KAT2B in LUAD and LUSC. The method used was as follows: i) Select the pan-cancer option, then click on the Gene Differential Expression option and finally search for the target gene in the search box; ii) select the chart type, box plot; iii) select the data scale method, log2(FPKM + 0.01); and iv) select the cancer name on the pan-cancer table to browse the corresponding differential profile. It should be noted that the StarBase database does not provide patient demographic data, which is a limitation of the present study. All data was obtained from three separate trials. The enrichment of histone acetylation marks on H3K18ac, H4K8ac and H3K27ac within gene promoter regions was analyzed using the UCSC Genome Browser (https://genome.ucsc.edu/) and the human genome assembly GRCh38/hg38 (GSE16256) (16). The promoter region was defined as 2 kb upstream to 500 bp downstream of the transcription start site for each gene of interest.

The statistical data, which were reported as the mean ± SD, were examined using GraphPad Prism (version 7.0; Dotmatics). The differences between two groups were investigated using paired and unpaired Student's t-tests. One-way ANOVA was performed to compare differences between >2 groups, followed by Tukey's Honestly Significant Difference test to determine which specific group means were significantly different from each other. $P<0.05$ was considered to indicate a statistically significant difference.

Results

RNF123 is a critical mediator of NSCLC cell proliferation. The starBase database projected that RNF123 was weakly expressed in LUAD and LUSC samples (Fig. 1A). Concurrently, it was observed that RNF123 was significantly downregulated in lung cancer cells compared with BEAS-2B cells (Fig. 1B and C). Among the lung cancer cell lines, the RNF123 expression levels exhibited the most pronounced changes in A549 and H1975 cells, hence these two cell lines were chosen for subsequent investigation. To elucidate the role of RNF123 in controlling lung cancer cell malignant behaviors, RNF123 overexpression and knockdown were induced in A549 and H1975 cells. oe-RNF123 and sh-RNF123 transfection significantly elevated and reduced RNF123 expression in both A549 and H1975 cells, respectively (Fig. 1D and E). Functional experiments showed that RNF123 overexpression markedly inhibited A549 and H1975 cell viability (Fig. 1F), proliferation (Figs. 1G and S1A), migration (Figs. 1H and S1B) and invasion (Figs. 1I and S1C), while RNF123 knockdown had the inverse effects. Epithelial-mesenchymal transition (EMT) is a process linked to cancer metastasis (17). During EMT, the reciprocal loss of E-cadherin (an adhesion molecule maintaining epithelial integrity via cell-cell junctions) and gain of Vimentin (a mesenchymal cytoskeletal protein promoting motility and invasive morphology) creates an inverse profile that serves as a hallmark of EMT and a key biomarker for tumor metastasis (18). RNF123 upregulation decreased Vimentin expression levels and elevated E-cadherin expression levels in lung cancer cells, while RNF123 downregulation had the opposite effect (Fig. 1J). Collectively, RNF123 upregulation suppressed lung cancer cell malignant behaviors.

RNF123 knockdown reverses the inhibitory effects of STS on NSCLC cells. STS, a water-soluble derivative of TSIIA

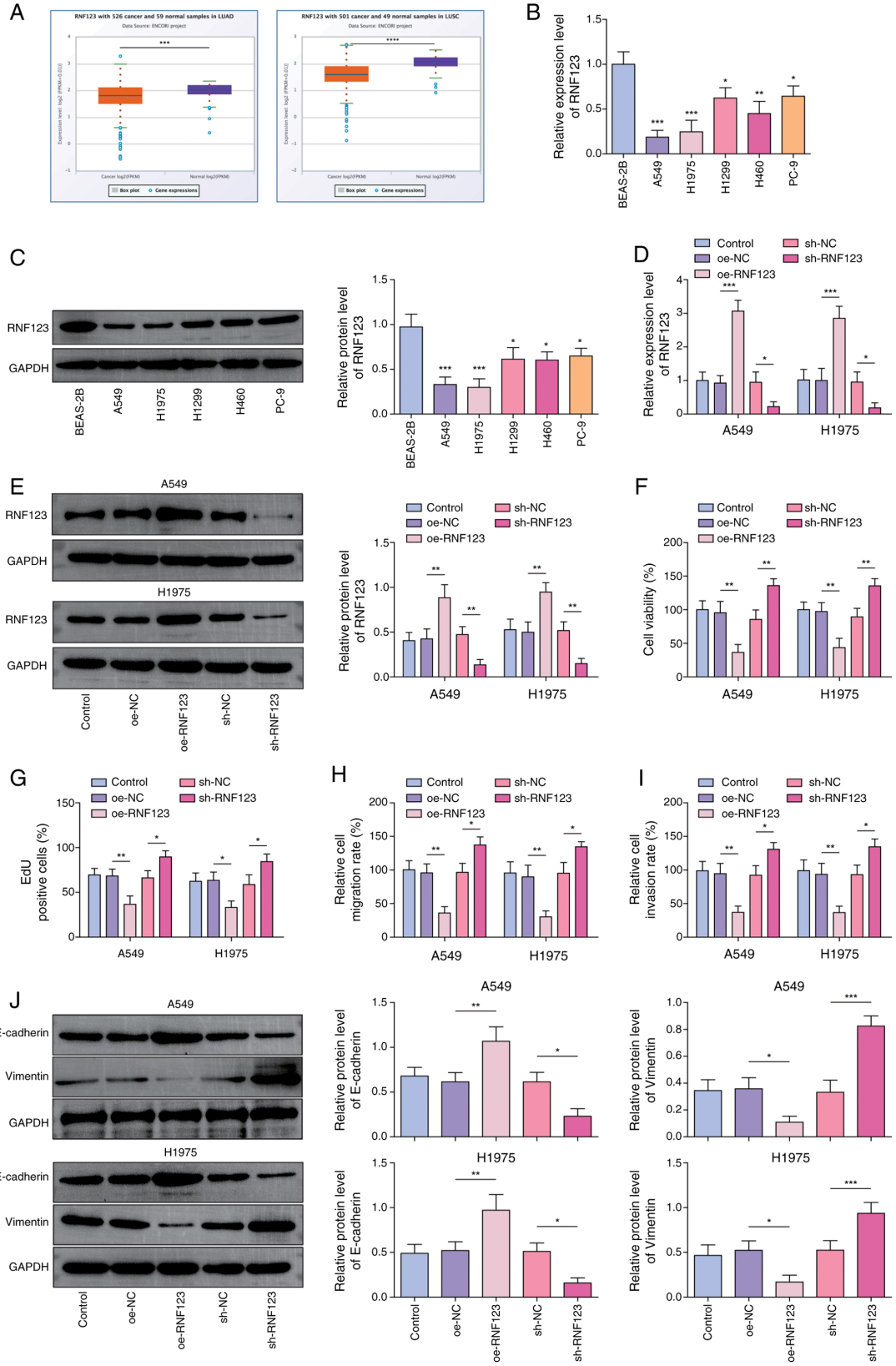

Figure 1. RNF123 is a critical mediator of non-small cell lung cancer cell proliferation, migration and invasion. (A) RNF123 expression in LUAD and LUSC was predicted using the starBase database. The mRNA and protein expression levels of RNF123 in lung cancer cells (A549, H1975, H1299, H460 and PC-9 cells) and the normal human bronchial epithelial cell line (BEAS-2B cells) were detected by (B) RT-qPCR and (C) western blotting, respectively. A549 and H1975 cells were transfected with oe-RNF123/sh-RNF123 or oe-NC/sh-NC. The mRNA and protein expression levels of RNF123 in cells were detected by (D) RT-qPCR and (E) western blotting, respectively. (F) Cell viability was examined using the Cell Counting Kit-8 assay. (G) The EdU assay was performed to determine cell proliferation. Cell (H) migration and (I) invasion were assessed using the Transwell assay in cells with RNF123 knockdown (sh-RNF123) or overexpression (oe-RNF123). Results are expressed as percentages relative to the control group (set as 100%). (J) E-cadherin and Vimentin protein expression levels in cells were measured by western blotting. Data are expressed as mean ± SD (n=3). *P<0.05, **P<0.01, ***P<0.001, ****P<0.0001. RNF123, RING finger protein 123; LUAD, lung adenocarcinoma; LUSC, lung squamous cell carcinoma; RT-qPCR, reverse transcription-quantitative PCR; oe, overexpression; sh, short hairpin RNA; NC, negative control; EdU, 5-ethynyl-20-deoxyuridine.

with a relative molecular mass of 396.39, dose-dependently reduced lung cancer cell viability, as determined using the CCK-8 assay (Fig. 2A). Additionally, STS elevated RNF123 expression levels in lung cancer cells in a dose-dependent manner (Fig. 2B). A concentration 40 μM STS was chosen for use in subsequent experiments due to its ability to reduce cell viability by ~50%. STS significantly upregulated RNF123 expression levels in A549 and H1975 cells; however, this effect was abrogated by sh-RNF123 transfection (Fig. 2C and D). In addition, STS treatment significantly reduced A549 and H1975 cell viability (Fig. 2E), proliferation (Figs. 2F and S2A), migration (Figs. 2G and S2B) and invasion (Figs. 2H and S2C), while RNF123 knockdown reversed these effects. Moreover, STS reduced Vimentin protein expression levels and elevated E-cadherin protein expression levels in A549 and H1975 cells. These changes in protein expression levels were reversed by RNF123 knockdown (Fig. 2I). Collectively, STS inhibited lung cancer cell malignant phenotypes potentially by upregulating RNF123 expression.

STS promotes H3K18ac modification of RNF123 in NSCLC cells. Histone acetylation alterations are linked to cancer progression (9). H3K18ac and H4K8ac expression levels were significantly reduced and H3K27ac expression levels were elevated in A549 and H1975 cells compared with BEAS-2B cells (Fig. 3A). As predicted by the UCSC database, H3K18ac, H4K8ac and H3K27ac were enriched in the RNF123 promoter region (Fig. S3). Given the pivotal role of histone acetylation in promoting gene transcription and the synchronous downregulation of RNF123, H3K18ac and H4K8ac expression levels in lung cancer cells, it was hypothesized that RNF123 may be modified by H3K18ac and H4K8ac. ChIP assay results demonstrated that H3K18ac was enriched in the RNF123 promoter, whereas enrichment of H4K8ac was not detected (Fig. 3B). Moreover, STS treatment significantly elevated H3K18ac and H4K8ac expression levels in A549 and H1975 cells (Fig. 3C). As confirmed by the ChIP assay results, STS promoted H3K18ac enrichment in the RNF123 promoter region but did not facilitate H4K8ac enrichment in the RNF123 promoter region (Fig. 3D). These results suggested that STS may increase the transcriptional activity of RNF123 through promoting H4K8ac enrichment in the RNF123 promoter.

STS promotes the H3K18ac modification and expression of RNF123 by upregulating the expression of KAT2B. KAT2B, an essential HAT epigenetic factor, serves as a biomarker for predicting prognosis in NSCLC (19,20). Herein, it was demonstrated that KAT2B was expressed at low levels in LUAD and LUSC using the starBase database (Fig. 4A). KAT2B expression levels were lower in A549 and H1975 cells compared with BEAS-2B cells (Fig. 4B and C). Notably, KAT2B expression in lung cancer cells was significantly increased by STS treatment (Fig. 4D and E). Furthermore, it was demonstrated that KAT2B was enriched in the RNF123 promoter region (Fig. 4F). Next, A549 and H1975 cells were transfected with oe-NC or oe-KAT2B, and the subsequent RT-qPCR and western blotting results showed that oe-KAT2B transfection significantly elevated the KAT2B expression levels (Fig. 4G and H). Additionally, KAT2B overexpression facilitated H3K18ac enrichment in the RNF123 promoter region (Fig. 4I). Moreover, KAT2B overexpression significantly elevated RNF123 expression levels in lung cancer cells (Fig. 4J and K). In conclusion, STS promoted RNF123 expression in lung cancer cells potentially by increasing the H3K18ac enrichment in the RNF123 promoter through upregulating KAT2B.

KAT2B knockdown reverses the inhibitory effects of STS on the malignant phenotypes of NSCLC cells. A549 and H1975 cells were subjected to STS treatment combined with sh-KAT2B or sh-NC transfection to elucidate the role of KAT2B in the STS-mediated anticancer effects. Initially, it was demonstrated that sh-KAT2B transfection significantly downregulated the KAT2B expression levels in A549 and H1975 cells (Fig. 5A and B). KAT2B expression levels in lung cancer cells were also significantly increased by STS administration and this upregulation was reversed by KAT2B knockdown (Fig. 5C-E). Furthermore, the knockdown of KAT2B counteracted the inhibitory effects of STS on cell viability (Fig. 5F), proliferation (Figs. 5G and S4A), migration (Figs. 5H and S4B) and invasion (Figs. 5I and S4C). It was also demonstrated that the promoting effect of STS on E-cadherin expression levels and the inhibitory effect on Vimentin expression levels in lung cancer cells were abolished following KAT2B knockdown (Fig. 5J). In summary, KAT2B knockdown neutralized the inhibitory effects of STS on the malignant phenotypes of lung cancer cells.

RNF123 overexpression reverses the effects of KAT2B knockdown on the STS-treated NSCLC cell malignant phenotypes. To investigate the interaction between KAT2B and RNF123 in the STS-mediated anticancer effects, A549 and H1975 cells treated with STS were co-transfected with RNF123 overexpression and KAT2B knockdown constructs. Co-transfection with oe-RNF123 rescued the suppressive effect of KAT2B knockdown on RNF123 expression levels in STS-treated A549 and H1975 cells (Fig. 6A and B). Additionally, RNF123 overexpression mitigated the sh-KAT2B-induced enhancement of the viability (Fig. 6C), proliferation (Figs. 6D and S5A), migration (Figs. 6E and S5B) and invasion (Figs. 6F and S5C) of STS-treated A549 and H1975 cells. Moreover, KAT2B knockdown reduced E-cadherin protein expression levels and elevated Vimentin expression levels in STS-treated A549 and H1975 cells, whereas RNF123 upregulation restored these effects (Fig. 6G). In conclusion, STS inhibited the lung cancer cell malignant phenotypes via modulating the KAT2B/RNF123 axis.

Discussion

Lung cancer is a major challenge to global health. According to global cancer statistics, there were 2.481 million new cases of lung cancer in 2022, accounting for 12.4% of all new cancer cases globally (1). Historically, the prognosis for patients with lung cancer has been poor (9). Over the past decade, significant advancements have been made in the field of lung cancer treatment, particularly in the areas of molecular targeted therapy and immunotherapy. For instance, targeted therapy against ROS proto-oncogene 1, receptor tyrosine kinase (ROS1) gene fusions have provided a new option for precision treatment for

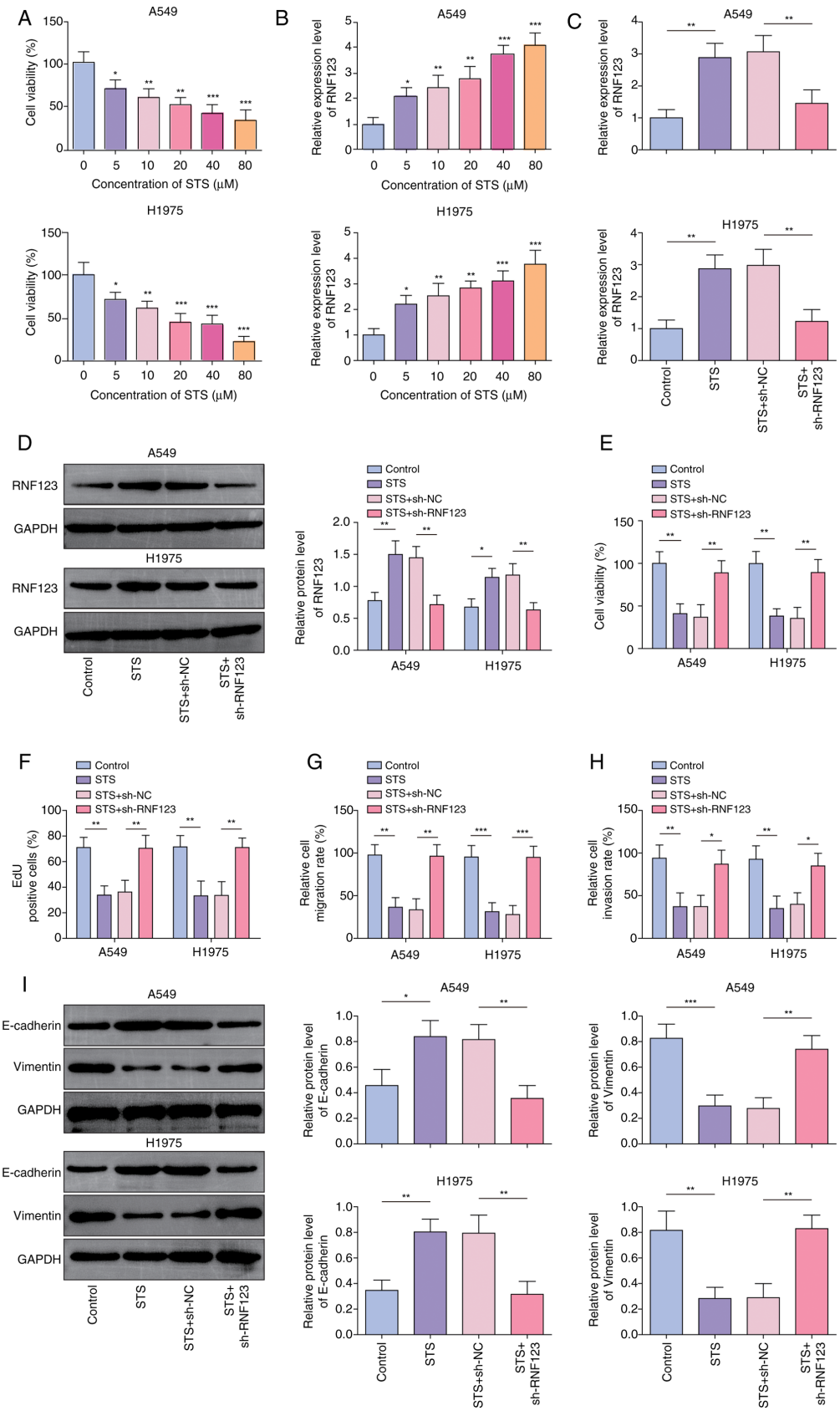

Figure 2. RNF123 knockdown reverses the inhibitory effects of STS on non-small cell lung cancer cells. A549 and H1975 cells were treated with 5, 10, 20, 40 and 80 μM STS for 24 h. (A) CCK-8 assay was employed to detect cell viability. (B) RT-qPCR was conducted to examined RNF123 mRNA expression level in cells. A549 and H1975 cells were treated with 40 μM STS for 24 h combined with sh-NC or sh-RNF123 transfection. The mRNA and protein expression levels of RNF123 in cells were detected by (C) RT-qPCR and (D) western blotting, respectively. (E) Cell viability was measured by CCK-8 assay. (F) EdU assay was performed to determine cell proliferation. Cell (G) migration and (H) invasion were detected by Transwell assay. Results are expressed as percentages relative to the control group (set as 100%). (I) Western blotting was performed to examine E-cadherin and Vimentin protein expression levels in cells. Data are expressed as mean ± SD (n=3). *P<0.05, **P<0.01, ***P<0.001. RNF123, RING finger protein 123; STS, sodium tanshinone IIA sulfate; CCK-8, Cell Counting Kit-8; RT-qPCR, reverse transcription-quantitative PCR; sh, short hairpin RNA; NC, negative control; EdU, 5-ethynyl-20-deoxyuridine.

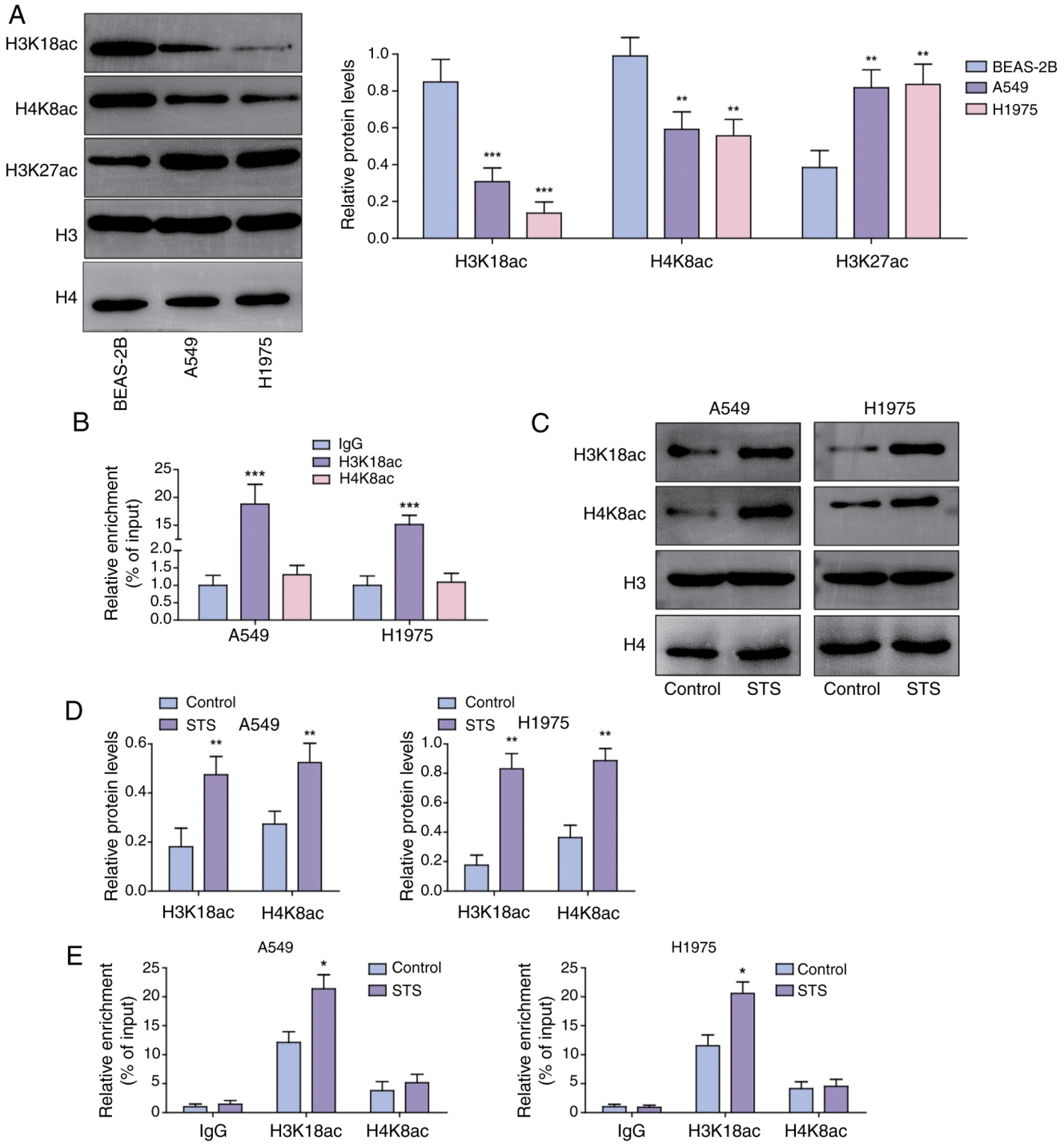

Figure 3. STS promotes H3K18ac modification of chromatin at the RNF123 locus in non-small cell lung cancer cells. (A) H3K18ac, H4K8ac and H3K27ac levels in A549, H1975 and BEAS-2B cells were assessed using western blotting. (B) The enrichment of H3K18ac and H4K8ac in the RNF123 promoter was analyzed by ChIP assay. A549 and H1975 cells were treated with 40 μM STS for 24 h. (C) H3K18ac and H4K8ac protein expression levels in cells were examined using western blotting and (D) semi-quantified. Histone acetylation signals were normalized to total histone H3 or H4 levels, respectively. (E) H3K18ac and H4K8ac enrichment in the RNF123 promoter was analyzed by ChIP assay. Data are expressed as mean ± SD (n=3). *P<0.05, **P<0.01, ***P<0.001. STS, sodium tanshinone IIA sulfate; RNF123, RING finger protein 123; H3K18ac, histone H3 lysine 18 acetylation; H4K8ac, histone H4 lysine 8 acetylation; H3K127ac, histone H3 lysine 27 acetylation; ChIP, chromatin immunoprecipitation.

patients with advanced NSCLC. ROS1-positive patients tend to be younger (median onset ~50 years) and are frequently non-smoking women with adenocarcinoma (3). However, despite these advancements, lung cancer remains the leading cause of cancer-related mortality (21). As a result, the discovery of novel therapeutic options to improve the survival of patients with lung cancer is required. The findings of the present study indicate that TSIIA suppresses lung cancer cell malignant phenotypes *in vitro* by increasing RNF123 expression levels through promoting KAT2B-mediated H3K18ac modification.

TSIIA, the predominant diterpenoid quinone derived from *Salvia miltiorrhiza*, has been utilized in China for

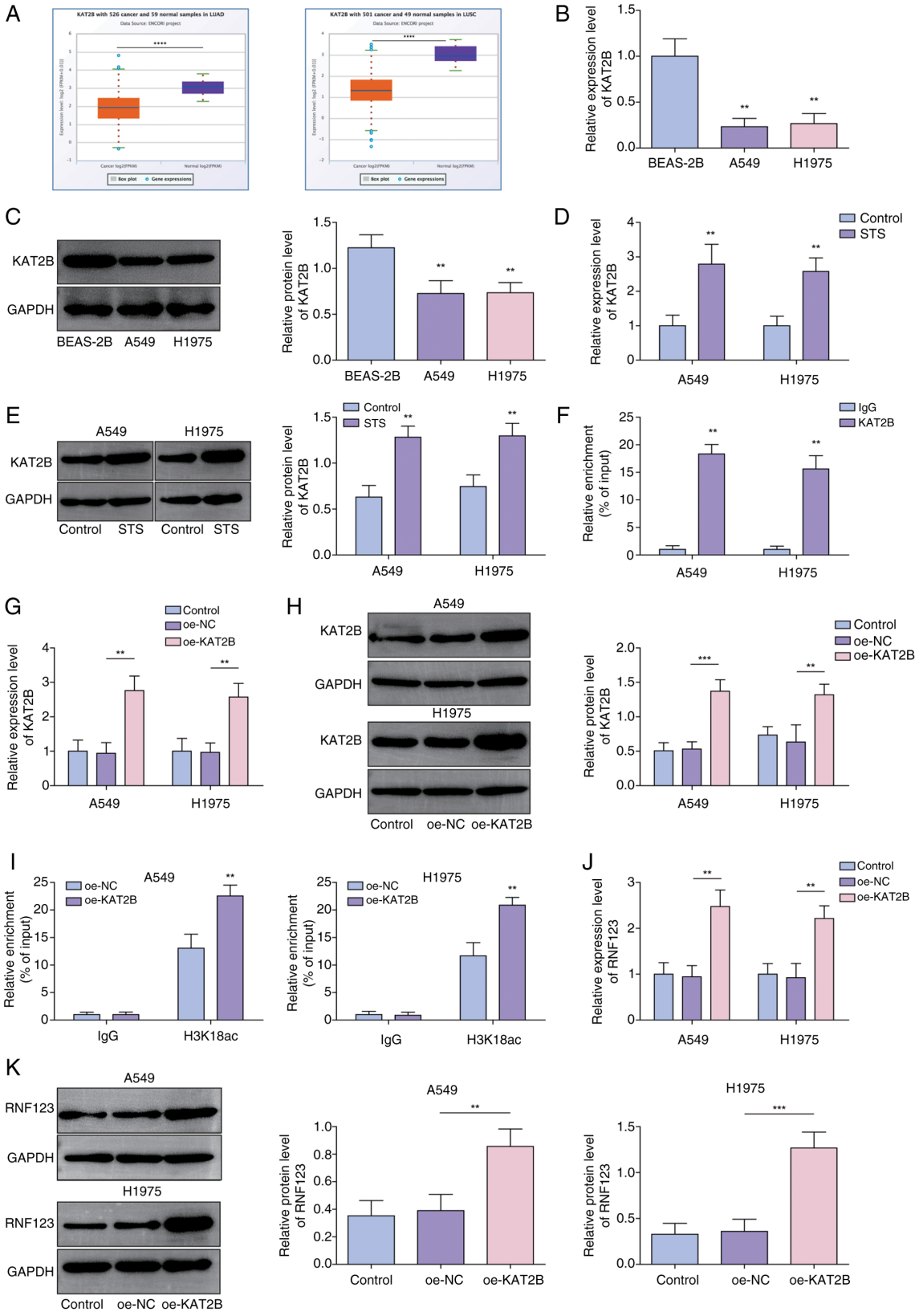

Figure 4. STS promotes the H3K18ac modification and expression of RNF123 by upregulating the expression of KAT2B. (A) KAT2B expression in LUAD and LUSC was predicted using the starBase database. The mRNA and protein expression levels of KAT2B in A549, H1975 and BEAS-2B cells were detected by (B) RT-qPCR and (C) western blotting, respectively. The mRNA and protein expression levels of KAT2B in A549 and H1975 cells after STS treatment were detected by (D) RT-qPCR and (E) western blotting, respectively. (F) The interaction between KAT2B and RNF123 promoter was analyzed by ChIP assay. A549 and H1975 cells were transfected with oe-NC or oe-KAT2B. The mRNA and protein expression levels of KAT2B in cells were detected by (G) RT-qPCR and (H) western blotting, respectively. (I) H3K18ac enrichment in the RNF123 promoter was analyzed by ChIP assay. The mRNA and protein levels of RNF123 in cells were detected by (J) RT-qPCR and (K) western blotting, respectively. Data are expressed as mean ± SD (n=3). **P<0.01, ***P<0.001, ****P<0.0001. STS, sodium tanshinone IIA sulfate; RNF123, RING finger protein 123; H3K18ac, histone H3 lysine 18 acetylation; KAT2B, lysine acetyltransferase 2B; LUAD, lung adenocarcinoma; LUSC, lung squamous cell carcinoma; RT-qPCR, reverse transcription-quantitative PCR; ChIP, chromatin immunoprecipitation; oe, overexpression; NC, negative control.

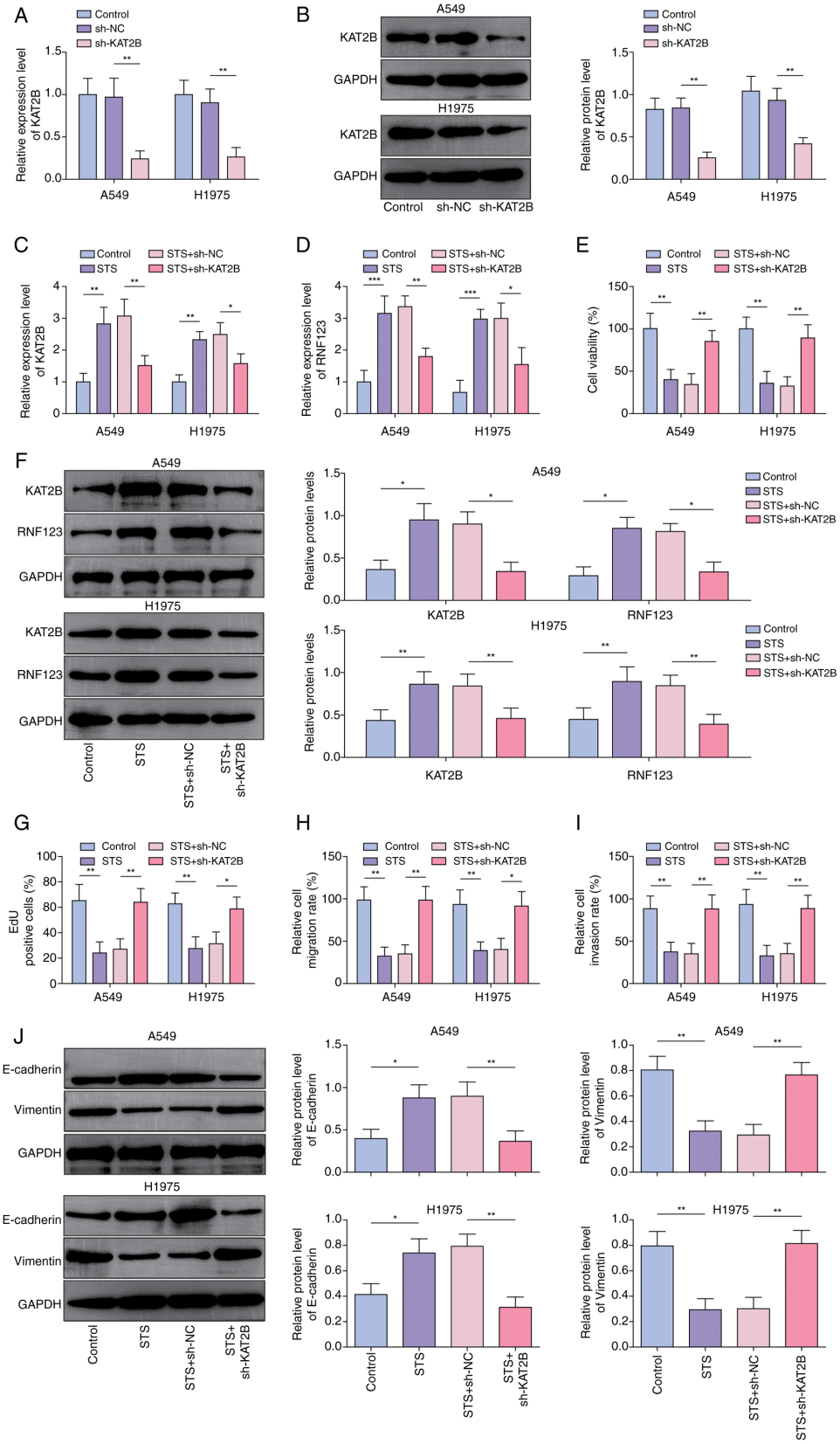

Figure 5. KAT2B knockdown reverses the inhibitory effects of STS on the malignant phenotypes of non-small cell lung cancer cells. KAT2B knockdown was induced in STS-treated A549 and H1975 cells. The mRNA and protein expression levels of KAT2B in A549 and H1975 cells after sh-NC or sh-KAT2B transfection were detected by (A) RT-qPCR and (B) western blotting, respectively. A549 and H1975 cells were treated with 40 μM STS for 24 h combined with sh-NC or sh-KAT2B transfection. The mRNA expression levels of (C) KAT2B and (D) RNF123 in cells were detected by RT-qPCR. (E) Cell viability was measured by Cell Counting Kit-8 assay. (F) The protein expression levels of RNF123 and KAT2B in cells were detected by western blotting. (G) EdU assay was performed to determine cell proliferation. Cell (H) migration and (I) invasion were detected by Transwell assay. Results are expressed as percentages relative to the control group (set as 100%). (J) E-cadherin and Vimentin protein levels in cells were examined by western blotting. Data are expressed as mean ± SD (n=3). *P<0.05, **P<0.01, ***P<0.001. KAT2B, lysine acetyltransferase 2B; STS, sodium tanshinone IIA sulfate; sh, short hairpin RNA; RT-qPCR, reverse transcription-quantitative PCR; NC, negative control; RNF123, RING finger protein 123; EdU, 5-ethynyl-20-deoxyuridine.

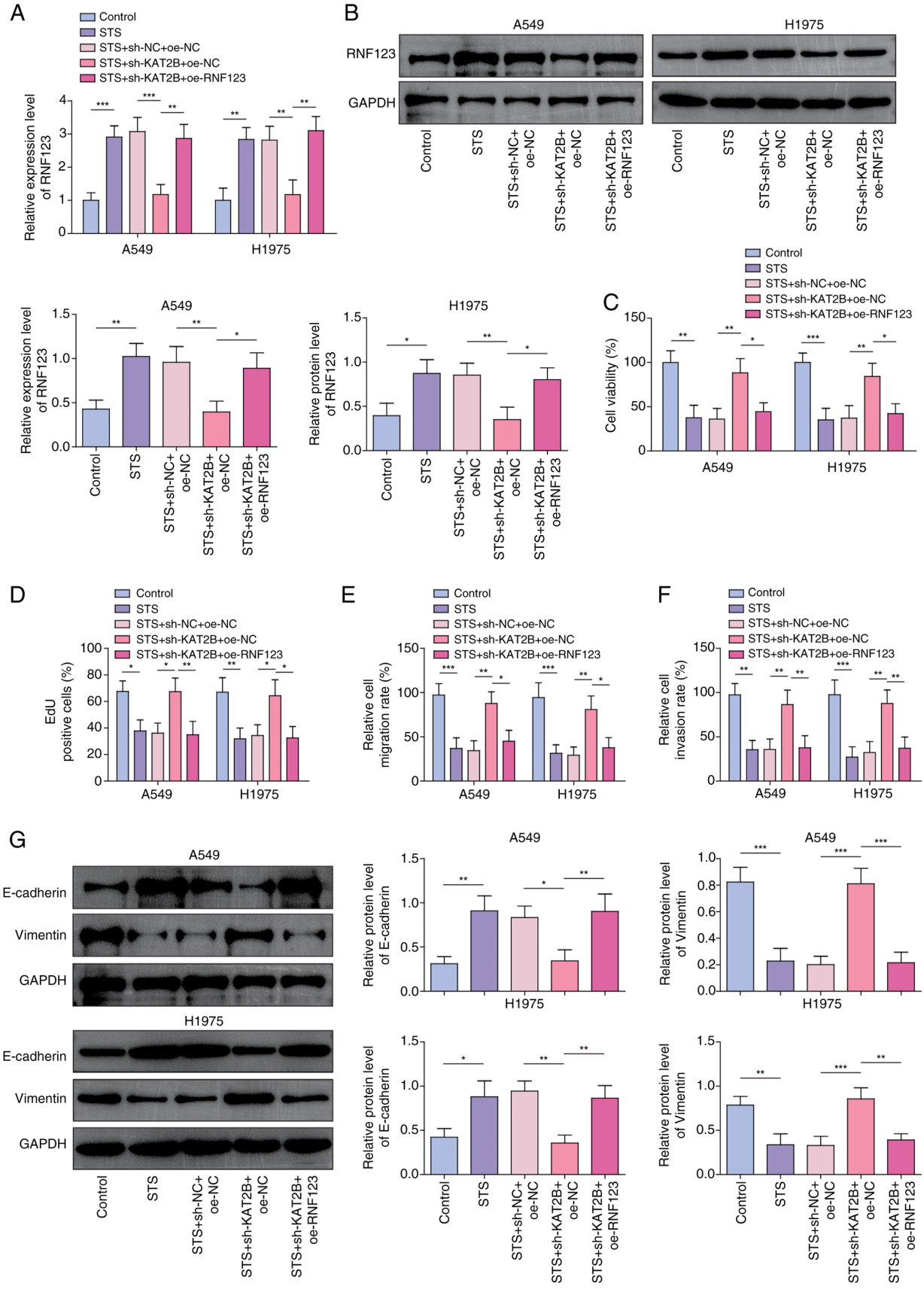

Figure 6. RNF123 overexpression reverses the effects of KAT2B knockdown on the malignant phenotypes of non-small cell lung cancer cells treated with STS. Both RNF123 overexpression and KAT2B knockdown were induced in STS-treated A549 and H1975 cells. The mRNA and protein expression levels of RNF123 in cells were detected by (A) RT-qPCR and (B) western blotting, respectively. (C) Cell viability was examined using Cell Counting Kit-8 assay. (D) EdU assay was performed to determine cell proliferation. Cell (E) migration and (F) invasion were assessed using Transwell assay. Results are expressed as percentages relative to the control group (set as 100%). (G) E-cadherin and Vimentin protein levels in cells were measured by western blotting. Data were expressed as mean ± SD (n=3). *P<0.05, **P<0.01, ***P< 0.001. STS, sodium tanshinone IIA sulfate; RNF123, RING finger protein 123; KAT2B, lysine acetyltransferase 2B; RT-qPCR, reverse transcription-quantitative PCR; NC, negative control; sh, short hairpin RNA; oe, overexpression; EdU, 5-ethynyl-20-deoxyuridine.

>2,000 years to treat cardiovascular disorders (22). In the past decade, research interest in the protective effects of TSIIA on cancer has increased. TSIIA suppresses EMT and migration in colorectal and gastric cancer cells (23,24), inhibits NSCLC proliferation through VEGF/VEGFR2 downregulation (25) and triggers SCLC apoptosis by upregulating Bax/Bcl-2 and reducing mitochondrial membrane potential (26). It has been previously shown that STS has potential in anticancer research as STS can effectively inhibit the cell viability and colony formation of NSCLC cells (6,7). Furthermore, STS has been reported to exert antitumor effects in the treatment of colorectal cancer (5). By targeting specific proteins and signaling pathways, STS may inhibit tumor proliferation and metastasis (25,27). However, the role of STS or TSIIA in controlling lung cancer migration, invasion and EMT is not well understood. The findings of the present study showed that STS treatment significantly inhibited lung cancer cell viability, proliferation, migration, invasion and EMT. TSIIA, a drug with multiple pharmacological effects, has a high efficiency, low toxicity and a natural source compared with chemotherapy drugs, and has significant potential clinical value (27). These findings provide a further foundation for TSIIA as a potential anti-lung cancer drug.

EMT is a critical process by which cancer cells acquire invasive and metastatic capabilities (17,18). In the present study, it was observed that treatment with STS significantly reduced the expression of the EMT marker, Vimentin, and increased the expression of E-cadherin in NSCLC cells. This suggests that STS may inhibit the invasiveness and metastatic potential of NSCLC cells by suppressing the EMT process. In recent years, EMT has been increasingly recognized not only as a biological process but also as a potential 'ecological process'. According to the nasopharyngeal carcinoma ecology theory proposed by Luo (28), cancer can be viewed as a multi-dimensional spatiotemporal 'unity of ecology and evolution' pathological ecosystem. Within this ecosystem, cancer cells interact dynamically with the tumor microenvironment and these interactions not only influence the biological behavior of cancer cells but may also shape tumor heterogeneity and invasiveness through ecological selection and evolutionary processes. During EMT, cancer cells exhibit mesenchymal characteristics, such as increased migratory and invasive abilities, which enable them to better adapt and survive in the competitive and resource-limited tumor microenvironment. This adaptive change can be seen as an ecological strategy that helps cancer cells gain a survival advantage (28). Moreover, EMT-associated cancer cells may interact dynamically with surrounding stromal cells (such as cancer-associated fibroblasts and immune cells) through the secretion of cytokines and exosomes, thereby further promoting tumor progression (17,28).

Ubiquitin E3 ligases serve a key role in normal human cells by regulating protein ubiquitination and degradation, which is a necessary metabolic activity for life (29). The E3-ligase, RNF123, has been reported to act as a tumor suppressor (13). Iida *et al* (30) demonstrated that RNF123 reduces melanoma proliferation by processing NF-κB1 p105 into p50. Furthermore, RNF123 is downregulated in aggressive glioblastoma and its downregulation is associated with a poor prognosis (14). However, to the best of our knowledge, the potential mechanism of action of RNF123 in lung cancer has not been previously reported. The results of the present study showed that RNF123 was expressed at low levels in lung cancer cells and its overexpression inhibited the lung cancer cell malignant phenotypes. Notably, it was also demonstrated that STS increased the RNF123 expression levels in lung cancer cells and RNF123 knockdown abolished the STS-induced inhibition of lung cancer cell malignant phenotypes. Collectively, the results suggested that STS inhibited lung cancer cell malignant phenotypes by increasing RNF123 expression levels.

Histone acetylation is an important component of transcriptional regulation, which depends on the balance of HAT and HDAC activities (31). The dysregulation of histone acetylation modifications promotes the development of human malignant tumors (9). The findings of the present study demonstrated that the H3K18ac and H4K8ac expression levels were significantly reduced and the H3K27ac expression levels were elevated in lung cancer cells. Moreover, H3K18ac and H4K8ac were enriched in the RNF123 promoter. As previously reported, TSIIA prevents cerebral ischemia reperfusion injury by regulating H3K18ac and H4K8ac (12). In the present study, STS increased the H3K18ac and H4K8ac expression levels in lung cancer cells. Additionally, STS facilitated H3K18ac enrichment in the RNF123 promoter. Collectively, the results of the present study indicated that STS increased RNF123 expression levels in lung cancer cells by promoting H3K18ac enrichment in the RNF123 promoter. KAT2B is a HAT that acetylates specific lysine residues in histones and therefore primarily serves a role in regulating chromatin remodeling, which is a key regulatory factor in signal transduction during the occurrence of numerous diseases, including cancer (32). KAT2B is an immune infiltration-associated biomarker that predicts prognosis in patients with NSCLC (20). The findings of the present study showed that KAT2B was expressed at low levels in lung cancer and STS increased KAT2B expression levels in lung cancer cells. Notably, KAT2B increased RNF123 expression levels in lung cancer cells by increasing the H3K18ac modification in chromatin at the RNF123 locus. Furthermore, KAT2B knockdown reversed the STS-induced inhibition of lung cancer cell malignant phenotypes. Moreover, RNF123 upregulation abrogated the effects of KAT2B knockdown on STS-treated lung cancer cell malignant phenotypes. These findings may be significant for NSCLC treatment as RNF123 was shown to suppress NSCLC proliferation and cellular activity in A549 and H1975 NSCLC cell lines, potentially emerging as a new target for treatment. STS inhibited NSCLC by upregulating RNF123 expression through the KAT2B/H3K18ac pathway, presenting a potential new treatment strategy. The low toxicity and lack of side effects of STS make it a promising therapy, potentially improving patient outcomes (27). The present study may offer valuable insights and highlight the clinical potential of this treatment against NSCLC.

However, there are a number of limitations of the present study. At present, the hypothesis that Tanshinone IIA targets RNF123 to inhibit NSCLC cell proliferation, migration and invasion via KAT2B-mediated H3K18ac modification has only been preliminarily verified at the cellular level and further confirmation requires animal and clinical experiments. Additionally, it was demonstrated that STS has effects on the H3K18ac

acetylation modification level; however, whether it also affects other acetylation modification levels and whether it is regulated by other acetylases requires further investigation. Although the present study preliminarily revealed that STS inhibits EMT by regulating RNF123 expression through KAT2B-mediated H3K18ac modification, the detailed molecular mechanisms still need further investigation. Specifically, whether TSIIA regulates other epigenetic modifications or signaling pathways to influence the EMT process should be explored. Moreover, the lack of patient demographic data from StarBase is a limitation of the present study, as it restricts the comprehensive understanding of the clinical relevance of RNF123 and KAT2B in lung cancer. By integrating the tumor ecology theory proposed by Luo (28), future studies could employ multidimensional approaches (such as single-cell sequencing and spatial transcriptomics) to comprehensively analyze the spatiotemporal dynamics of the EMT process within the tumor ecosystem. This will help us better understand the complexity of tumors and provide new insights for developing precision medicine strategies.

Taken together, the results of the present study demonstrated that STS inhibited the lung cancer cell malignant phenotypes by upregulating RNF123 through promoting KAT2B-mediated H3K18ac modification of chromatin at the RNF123 locus. TSIIA may have potential for the treatment of lung cancer in the future and RNF123 may serve as an important target for the anticancer actions of TSIIA.

Acknowledgements

Not applicable.

Funding

Work was funded by the grant provided by the China Medicine Education Association named 'Construction of three-generation sequencing database and data analysis platform' (grant no. 2022KTZ017).

Availability of data and materials

The data generated in the present study may be requested from the corresponding author.

Authors' contributions

The study and figures were designed by YH and KC. YH and YZ conducted the experiments and interpreted the results with JZ. YH, KC and JZ supervised the study. Bioinformatics analysis was performed by YH. Funding was obtained by KC. YH wrote the manuscript draft. All authors read and approved the final version of the manuscript. YH, YZ, JZ and KC confirm the authenticity of all the raw data.

Ethics approval and consent to participate

Not applicable.

Patient consent for publication

Not applicable.

Competing interests

The authors declare that they have no competing interests.

References

1. Siegel RL, Miller KD, Fuchs HE and Jemal A: Cancer statistics, 2022. CA Cancer J Clin 71: 7-33, 2022.
2. Feng J, Li J, Qie P, Li Z, Xu Y and Tian Z: Long non-coding RNA (lncRNA) PGM5P4-AS1 inhibits lung cancer progression by up-regulating leucine zipper tumor suppressor (LZTS3) through sponging microRNA miR-1275. Bioengineered 12: 196-207, 2021.
3. Bade BC and Dela Cruz CS: Lung cancer 2020: Epidemiology, etiology, and prevention. Clin Chest Med 41: 1-24, 2020.
4. Yang LJ, Jeng CJ, Kung HN, Chang CC, Wang AG, Chau GY, Don MJ and Chau YP: Tanshinone IIA isolated from *Salvia miltiorrhiza* elicits the cell death of human endothelial cells. J Biomed Sci 12: 347-361, 2005.
5. Liu L, Gao H, Wen T, Gu T, Zhang S and Yuan Z: Tanshinone IIA attenuates AOM/DSS-induced colorectal tumorigenesis in mice via inhibition of intestinal inflammation. Pharm Biol 59: 89-96, 2021.
6. Gao F, Li M, Liu W and Li W: Inhibition of EGFR signaling and activation of mitochondrial apoptosis contribute to tanshinone IIA-mediated tumor suppression in non-small cell lung cancer cells. Onco Targets Ther 13: 2757-2769, 2020.
7. Wang B, Zou F, Xin G, Xiang BL, Zhao JQ, Yuan SF, Zhang XL and Zhang ZH: Sodium tanshinone IIA sulphate inhibits angiogenesis in lung adenocarcinoma via mediation of miR-874/eEF-2K/TG2 axis. Pharm Biol 61: 868-877, 2023.
8. Dawson MA and Kouzarides T: Cancer epigenetics: From mechanism to therapy. Cell 150: 12-27, 2012.
9. Guo P, Chen W, Li H, Li M and Li L: The histone acetylation modifications of breast cancer and their therapeutic implications. Pathol Oncol Res 24: 807-813, 2018.
10. Cheng Z, Li X, Hou S, Wu Y, Sun Y and Liu B: K-Ras-ERK1/2 accelerates lung cancer cell development via mediating $H3^{K18ac}$ through the MDM2-GCN5-SIRT7 axis. Pharm Biol 57: 701-709, 2019.
11. Chen G, Zhu X, Li J, Zhang Y, Wang X, Zhang R, Qin X, Chen X, Wang J, Liao W, *et al*: Celastrol inhibits lung cancer growth by triggering histone acetylation and acting synergically with HDAC inhibitors. Pharmacol Res 185: 106487, 2022.
12. Ma H, Hu ZC, Long Y, Cheng LC, Zhao CY and Shao MK: Tanshinone IIA microemulsion protects against cerebral ischemia reperfusion injury via regulating H3K18ac and H4K8ac in vivo and in vitro. Am J Chin Med 50: 1845-1868, 2022.
13. Gulei D, Drula R, Ghiaur G, Buzoianu AD, Kravtsova-Ivantsiv Y, Tomuleasa C and Ciechanover A: The tumor suppressor functions of ubiquitin ligase KPC1: From cell-cycle control to NF-κB regulator. Cancer Res 83: 1762-1767, 2023.
14. Wang X, Bustos MA, Zhang X, Ramos RI, Tan C, Iida Y, Chang SC, Salomon MP, Tran K, Gentry R, *et al*: Downregulation of the ubiquitin-E3 ligase RNF123 promotes upregulation of the NF-κB1 target SerpinE1 in aggressive glioblastoma tumors. Cancers (Basel) 12: 1081, 2020.
15. Livak KJ and Schmittgen TD: Analysis of relative gene expression data using real-time quantitative PCR and the 2(-Delta Delta C(T)) method. Methods 25: 402-408, 2001.
16. Heintzman ND, Hon GC, Hawkins RD, Kheradpour P, Stark A, Harp LF, Ye Z, Lee LK, Stuart RK, Ching CW, *et al*: Histone modifications at human enhancers reflect global cell-type-specific gene expression. Nature 459: 108-112, 2009.
17. Hashemi M, Arani HZ, Orouei S, Fallah S, Ghorbani A, Khaledabadi M, Kakavand A, Tavakolpournegari A, Saebfar H, Heidari H, *et al*: EMT mechanism in breast cancer metastasis and drug resistance: Revisiting molecular interactions and biological functions. Biomed Pharmacother 155: 113774, 2022.
18. Serrano-Gomez SJ, Maziveyi M and Alahari SK: Regulation of epithelial-mesenchymal transition through epigenetic and post-translational modifications. Mol Cancer 15: 18, 2016.
19. Hou YS, Wang JZ, Shi S, Han Y, Zhang Y, Zhi JX, Xu C, Li FF, Wang GY and Liu SL: Identification of epigenetic factor KAT2B gene variants for possible roles in congenital heart diseases. Biosci Rep 40: BSR20191779, 2020.
20. Zhou X, Wang N, Zhang Y, Yu H and Wu Q: KAT2B is an immune infiltration-associated biomarker predicting prognosis and response to immunotherapy in non-small cell lung cancer. Invest New Drugs 40: 43-57, 2022.

21. Megyesfalvi Z, Gay CM, Popper H, Pirker R, Ostoros G, Heeke S, Lang C, Hoetzenecker K, Schwendenwein A, Boettiger K, *et al*: Clinical insights into small cell lung cancer: Tumor heterogeneity, diagnosis, therapy, and future directions. CA Cancer J Clin 73: 620-652, 2023.
22. Xu S and Liu P: Tanshinone II-A: New perspectives for old remedies. Expert Opin Ther Pat 23: 149-153, 2013.
23. Song Q, Yang L, Han Z, Wu X, Li R, Zhou L, Liu N, Sui H, Cai J, Wang Y, *et al*: Tanshinone IIA inhibits epithelial-to-mesenchymal transition through hindering β-arrestin1 mediated β-catenin signaling pathway in colorectal cancer. Front Pharmacol 11: 586616, 2020.
24. Yuan F, Zhao ZT, Jia B, Wang YP and Lei W: TSN inhibits cell proliferation, migration, invasion, and EMT through regulating miR-874/HMGB2/β-catenin pathway in gastric cancer. Neoplasma 67: 1012-1021, 2020.
25. Xie J, Liu J, Liu H, Liang S, Lin M, Gu Y, Liu T, Wang D, Ge H and Mo SL: The antitumor effect of tanshinone IIA on anti-proliferation and decreasing VEGF/VEGFR2 expression on the human non-small cell lung cancer A549 cell line. Acta Pharm Sin B 5: 554-563, 2015.
26. Cheng CY and Su CC: Tanshinone IIA may inhibit the growth of small cell lung cancer H146 cells by up-regulating the Bax/Bcl-2 ratio and decreasing mitochondrial membrane potential. Mol Med Rep 3: 645-650, 2010.
27. Fang ZY, Zhang M, Liu JN, Zhao X, Zhang YQ and Fang L: Tanshinone IIA: A review of its anticancer effects. Front Pharmacol 11: 611087, 2021.
28. Luo W: Nasopharyngeal carcinoma ecology theory: Cancer as multidimensional spatiotemporal 'unity of ecology and evolution' pathological ecosystem. Theranostics 13: 1607-1631, 2023.
29. Berndsen CE and Wolberger C: New insights into ubiquitin E3 ligase mechanism. Nat Struct Mol Biol 21: 301-307, 2014.
30. Iida Y, Ciechanover A, Marzese DM, Hata K, Bustos M, Ono S, Wang J, Salomon MP, Tran K, Lam S, *et al*: Epigenetic regulation of KPC1 ubiquitin ligase affects the NF-κB pathway in melanoma. Clin Cancer Res 23: 4831-4842, 2017.
31. Shvedunova M and Akhtar A: Modulation of cellular processes by histone and non-histone protein acetylation. Nat Rev Mol Cell Biol 23: 329-349, 2022.
32. Li L, Zhang J and Cao S: Lysine acetyltransferase 2B predicts favorable prognosis and functions as anti-oncogene in cervical carcinoma. Bioengineered 12: 2563-2575, 2021.

Copyright © 2025 He et al. This work is licensed under a Creative Commons Attribution-NonCommercial-NoDerivatives 4.0 International (CC BY-NC-ND 4.0) License.